Energy &
Environmental
Science

ROYAL SOCIETY
OF CHEMISTRY

Effect of electrolyte on the nanostructure of the solid electrolyte interphase (SEI) and performance of lithium metal anodes

SCHOLARONE™
Manuscripts

Effect of electrolyte on the nanostructure of the solid electrolyte interphase (SEI) and performance of lithium metal anodes

Sunhyung Jurng, Zachary L. Brown, Jiyeon Kim, and Brett L. Lucht

Department of Chemistry, University of Rhode Island, Kingston, Rhode Island 02881, USA

Abstract

Developing electrolytes that enable commercially viable lithium metal anodes for rechargeable lithium batteries remains challenging, despite recent exhaustive efforts. Electrolytes of similar composition, yet different structure, have been investigated to understand key mechanisms for improving the cycling performance of lithium metal anodes. Specifically, the electrolytes investigated include $LiPF_6$, $LiBF_4$, lithium bis(oxalato)borate (LiBOB), and lithium difluoro(oxalato)borate (LiDFOB) dissolved in a mixture of ethylene carbonate (EC) and ethyl methyl carbonate (EMC). There is a remarkable difference in the cycling performance of 1.2 M LiDFOB in EC:EMC (3:7) compared to 0.6 M $LiBF_4$ + 0.6 M LiBOB in EC:EMC (3:7), despite the effectively equivalent chemical composition. The LiDFOB electrolyte has significantly better cycling performance. Furthermore, the chemical compositions of the SEI generated on the lithium metal electrode from the two electrolytes are very similar, especially after the 1st plating, suggesting that the chemical composition of the SEI may not be the primary source for the difference in cycling performance. Ex-situ transmission electron microscopy (TEM) reveals that the difference in cycling performance can be traced to the presence of nanostructured LiF particles in the SEI from the LiDFOB electrolyte. It is proposed that the capping ability of the oxalate moiety from LiDFOB, in combination with simultaneous generation of LiF, leads to generation of uniform and evenly distributed nanostructured LiF particles. The presence of nanostructured LiF in the SEI results in uniform diffusion field gradients on the lithium electrode which leads to improved cycling performance. The proposed mechanism not only provides insight for improving lithium metal anodes for batteries, but also expands upon the understanding of the role of LiF in the SEI on graphite electrodes in commercial lithium ion batteries. A superior understanding of the structure and function of the SEI will facilitate the development of next-generation energy storage systems.

1. Introduction

Lithium metal is a promising negative electrode material for future high-energy batteries for consumer electronics and electric vehicles. Lithium metal anodes have a very high theoretical specific capacity of 3,860 mAh g^{-1}, extremely low negative potential (-3.04 V *vs.* standard hydrogen electrode) and low gravimetric density of 0.534 g cm^{-3}. Thus, application of lithium metal to secondary lithium batteries has been investigated intensively.[1, 2] However several barriers exist in commercializing lithium metal anodes, including the formation of lithium dendrites, safety risks caused by dendritic lithium, and low Coulombic efficiency.

Since lithium metal reacts with most common electrolytes, a solid electrolyte interphase (SEI)[3] is generated from the decomposition of the electrolyte on the lithium metal anode during the plating process. The SEI stabilizes lithium metal and prevents further reaction with the electrolyte. While the SEI on lithiated graphite electrodes used in commercial lithium ion batteries has reasonable stability to afford long term cycling performance, a stable SEI on lithium metal anodes has not been observed. The instability of the SEI on lithium metal leads to poor efficiency and irreversible consumption of lithium. Thus, the generation of a thin and stable SEI for lithium metal anodes is critical. Variation of the electrolyte used with lithium metal anodes has been reported to result in significant changes to cycling efficiency and lithium dendrite growth. These variations in electrolyte include, but are not limited to, solid-state or polymer electrolytes[4-6], concentrated electrolytes[7], ionic liquids[8], and electrolyte additives[9-11]. At this time, an effective electrolyte for lithium metal anodes still remains elusive. However, establishing a better understanding of how electrolyte modifications results in improved performance of lithium metal anodes is critical for the systematic design of the next generation of electrolytes.

Development of carbonate electrolytes for lithium metal anodes is desired, given their versatile properties,[12] such as a high dielectric constant, chemical stability, and wide electrochemical window.[10, 13-15] Recent work has demonstrated that LiF is a key SEI component for enabling rechargeable lithium metal batteries in carbonate electrolytes.[13, 16-19] However, LiF is a common component of nearly every SEI generated on the surface of the lithium metal anode, regardless of electrochemical performance.[20] Therefore, the mechanism of LiF generation from the electrolyte and the structure of the LiF particles must strongly influence the electrochemical performance of lithium metal. In addition, the importance of the morphology or nanostructure of SEI components, including LiF, has been proposed for decades[21, 22], however, direct evidence has not been reported. Herein, a unique mechanism for the generation of nanostructured LiF is proposed along with a mechanistic rationale for the improved electrochemical performance of an SEI on lithium metal containing nanostructured LiF. The results suggest the significance of the SEI nanostructure to electrochemical performance of battery electrodes, as previously proposed with limited experimental justification.[23-25] This finding furthers the understanding of the nature of lithium metal anode and provides insight regarding the rational design of the SEI for electrode materials in lithium-ion batteries. In particular, this insight can facilitate the development of

commercial graphite or silicon anodes, where the nature of the SEI plays a crucial role in determining electrochemical performance.

The effect of lithium salt on the performance of lithium metal anodes has been investigated. Lithium tetrafluoroborate ($LiBF_4$), lithium bis(oxalato)borate (LiBOB) and lithium difluoro(oxalato)borate (LiDFOB) (Fig. 1) have been compared to lithium hexafluorophosphate ($LiPF_6$) in a common blend of carbonate solvents, ethylene carbonate (EC) and ethyl methyl carbonate (EMC) which is widely used commercially.[26] In order to minimize reactivity of cell components with the electrolyte, $LiFePO_4$/Cu cells[27] (Fig. S1) were used to investigate the SEI generated by each electrolyte on lithium metal anodes.[28] The 1.2 M LiDFOB in EC:EMC (3:7) electrolyte was observed to dramatically improve the plating and stripping performance of lithium metal anodes, while the effectively identical chemical composition, 0.6 M $LiBF_4$ + 0.6 M LiBOB in EC:EMC (3:7) had poor platting and stripping performance. It is proposed that the capping ability of the oxalate moiety from LiDFOB, in combination with simultaneous generation of LiF, leads to optimal growth of the nanostructured LiF particles. The presence of nanostructured LiF in the SEI results in uniform diffusion field gradients on the lithium anode which leads to improved cycling performance.

2. Experimental

2.1. Coin Cell Preparation

2032-type coin cells containing $LiFePO_4$ and copper foil electrodes were used for electrochemical testing. $LiFePO_4$/Cu cells were assembled for each electrolyte (135 μL), consisting of a $LiFePO_4$ positive electrode (13.7 mm diameter, MTI Corporation), a PP/PE/PP separator (19 mm diameter, Celgard 2325) and a copper foil negative electrode (19 mm diameter, MTI Corporation). The $LiFePO_4$ cathodes are composed of 91 % active material and 9 % of PVDF binder and conductive carbon. The average active mass loading and areal capacity of $LiFePO_4$ cathodes is 10.5 mg cm^{-2} and 1.75 mAh cm^{-2}, respectively. The copper foil was cleaned with 1 M HCl solution followed by sonication with distilled water and hexane. Both $LiFePO_4$ and copper foil electrodes were punched to a specific diameter, and dried at 110°C under vacuum overnight before cell assembly. $LiFePO_4$/Cu cells were assembled in an argon glove box (M-Braun) with oxygen and water contents < 1 ppm. The electrolytes investigated are: 1.2 M $LiPF_6$ in EC:EMC ($LiPF_6$ electrolyte), 1.2 M $LiBF_4$ in EC:EMC ($LiBF_4$ electrolyte), 1.2 M LiDFOB in EC:EMC (LiDFOB electrolyte), the mixture of 0.6 M $LiBF_4$ and 0.6 M LiBOB in EC:EMC ($LiBF_4$+LiBOB electrolyte), and 0.6 M LiBOB in EC:EMC (LiBOB electrolyte). The mixture of ethylene carbonate and ethyl methyl carbonate (EC:EMC=3:7, volume:volume) is the solvent for all electrolytes. All electrolyte components (salts and solvents) were supplied from a commercial supplier as battery grade with less than 50 ppm water, and used as received.

2.2. Electrochemical Testing

Galvanostatic cycling (lithium plating/stripping) of $LiFePO_4$/Cu cells was conducted using an Arbin BT2000 battery cycler at room temperature (25°C) in a constant temperature oven. The cycling procedure of $LiFePO_4$/Cu cells consists of plating lithium at a rate of 0.1 mA/cm^2 with subsequent cycling at a rate of 0.5 mA/cm^2, within a voltage cut-off of 2.0-4.0 V *vs.* Li/Li$^+$. A 3-hour rest period was inserted at the beginning of each cycling protocol to ensure uniform wetting of all cell components.

2.3. X-ray Photoelectron Spectroscopy (XPS)

XPS measurements were conducted with a K-alpha spectrometer (Thermo Scientific) using Al Kα radiation (hν = 1486.6 eV) under ultra-high vacuum ($< 1 \times 10^{-12}$ atm). The spot size and pass energy were 400 μm in diameter and 60 eV respectively. After cycling, the $LiFePO_4$/Cu cells were allowed to equilibrate for 48 hours and disassembled in an argon glove box. Lithium electrodes were washed with a EC:EMC (3:7) solution followed by only EMC to remove the salt residue and EC, dried overnight under vacuum (approx. 3×10^{-3} atm), and then transferred in an air-free container from the glove box to the XPS chamber. The binding energy scale was corrected using the LiF peak (685 eV) in the F 1s spectra. Relative atomic concentrations were determined from integration of the XPS peaks, accounting for respective atomic sensitivity factors.

2.4. Transmission Electron Microscopy (TEM)

TEM measurements were conducted with a JEOL JEM-2100F at 200 kV, equipped with a LaB_6 electron emission source. Pelco copper TEM grids, 500 mesh, were placed on a copper foil electrode and assembled with $LiFePO_4$, as described above. Approximately 15% of the lithium from the $LiFePO_4$ electrode was plated at constant current with voltage of approximately 3.45 V, characteristic of the $LiFePO_4$ electrode vs. Li/Li$^+$. and allowed to equilibrate for 48 hours. After cell equilibration, the TEM grid was collected and washed with EMC and dried under vaccum ($< 3 \times 10^{-3}$ atm). After drying, the grid was transferred to the TEM chamber without air exposure using a Cryo-Transfer holder and a sealable Aldrich AtmosBag. Energy-dispersive X-ray spectroscopy (EDX, INCAx-act, Oxford Instrument) was also conducted to analyze the element composition using beam diameters between 10 – 25 nm.

3. Results and Discussion

3.1. Electrochemistry

The cycling performance of these cells is depicted with Coulombic efficiency versus cycle number (Fig. 1a) and the total amount of lithium stripped each cycle (Fig. 1b). The stripping capacity versus cycle number is also presented in supplementary Fig. S2. The cycling performance is clearly dependent upon the salt used in the electrolyte, suggesting that the salt is involved in either SEI formation or mossy lithium generation. The performance differences are easily discernible with the $LiFePO_4$/Cu cells since there is no excess lithium as there is for the Li/Li or Li/Cu cells (Fig. S1). Thus, lithium loss during plating and stripping is more dramatic for the $LiFePO_4$/Cu cells than in Li/Li symmetric cells. The cells cycled with the $LiBF_4$, LiBOB, and $LiBF_4$+LiBOB electrolytes have better initial capacity retention (Fig. S2b) and cycling efficiency than cells cycled with the $LiPF_6$ electrolyte, but retained capacity is insignificant after only 10 cycles. However, the cell cycled with the LiDFOB electrolyte has dramatically better efficiency and capacity retention over the first 50 cycles, maintaining >95% efficiency through the 50th cycle. It is noteworthy that the performance of the cell cycled with $LiBF_4$+LiBOB electrolyte is much worse than the cell cycled with LiDFOB electrolyte, despite the effectively equivalent chemical composition of the electrolytes (see the chemical structures depicted in Fig. 1), suggesting that the DFOB anion has a unique interaction with the lithium metal surface. In addition, variation of the LiDFOB salt concentration from 1.2 to 1.8 M resulted in only small changes in performance (Fig. S10).

The 1st plating and stripping cycle of lithium with the different electrolytes in $LiFePO_4$/Cu cells is provided in supplementary Fig. S2a. Significant changes in the stripping capacities are observed when comparing the electrochemical performance of all electrolytes. This suggests that either the quantity of electrolyte decomposition to generate a solid electrolyte interphase (SEI) is much greater for cells with poor first cycle efficiency or significant mossy lithium is generated resulting in poor stripping. All of the cells containing the alternative salts have better first cycle efficiency than cells containing $LiPF_6$ (25.1%).

Nyquist plots of Li/Li symmetric cells, in which lithium electrodes were generated from $LiFePO_4$/Cu cells cycled with the different electrolytes, are provided in supplementary Fig. S3. Upon the 10th plating, the overall impedance of cells is inversely related to the capacity retention ($LiPF_6$ > $LiBF_4$ > LiBOB ≈ $LiBF_4$+LiBOB > LiDFOB). The strong correlation suggests that cell performance is dominated by the plating and stripping of lithium on copper and not the $LiFePO_4$ electrode. Differences in the structure and stability of the SEI on the lithium metal are likely responsible for the differences in impedance and cycling performance.

Galvanostatic cycling results observed for Li/Li symmetric cells cycled with the different electrolytes are shown in supplementary Fig. S4. Except for the cell containing the LiDFOB

electrolyte (Fig. S4c), a rapidly increasing voltage is observed during both charge/discharge steps where the voltage limit (3.5 V) is reached in less than 50 cycles. This voltage increase is characteristic of a significant increase in the impedance of lithium electrodes in the cells during cycling.[7, 29] Upon reaching this voltage limit, lithium is no longer being cycled and the cells have reached "high impedance failure".[7, 29] Conversely, the cell containing the LiDFOB electrolyte demonstrates stable charge/discharge behavior for more than 2000 hours (250 cycles) and do not undergo impedance failure. This improvement in cycling confirms that observations with LiFePO$_4$/Cu are representative of behavior with Li/Li cells, i. e. the LiDFOB electrolyte improves the electrochemical performance of the lithium metal anode.[30-32]

3.2. Surface Film Analysis (XPS)

The surface of lithium metal was investigated with XPS. Spectra of the electrodes were acquired after the 1st and the 10th plating (Fig. 2). The spectra of the electrodes acquired after 15% of the available lithium was removed from LiFePO$_4$ (i. e. 15% state-of-charge) during the 1st plating are depicted in supplementary Fig. S5. The corresponding relative atomic concentrations from XPS spectra are provided in supplementary Fig. S6.

The C 1s spectrum of the lithium electrode plated with the LiPF$_6$ electrolyte contains peaks characteristic of Li$_2$CO$_3$ or lithium alkyl carbonates (290.3 eV) along with a C-O peak (286.8 eV).[20, 33-35] There are corresponding peaks at 531.8 and 533.5 eV in the O 1s spectra, which are characteristic of C=O and C-O, respectively[20, 33-35], supporting the presence of lithium alkyl carbonates and Li$_2$CO$_3$. The F 1s spectrum has an intense peak at 685 eV, characteristic of LiF[20, 33-35]. The XPS spectra do not change significantly upon prolonged cycling. The relative atomic concentrations calculated from corresponding XPS spectra (Fig. S6), illustrate that the surface of the lithium electrode plated with the LiPF$_6$ electrolyte has high concentrations of inorganic species, especially LiF, as can be observed in the F 1s spectra.

The surface of the lithium electrode plated with the LiBF$_4$ electrolyte has much less Li$_2$CO$_3$ or lithium alkyl carbonates (C 1s) compared to the lithium electrode plated with the LiPF$_6$ electrolyte, however, an intense C-O peak is observed. This C-O peak grows notably after prolonged cycling. In the F 1s spectrum, the LiF peak (685 eV) is present during the very early stage of plating (15% of lithium from the LiFePO$_4$ electrode, Fig. S5), however, the additional peaks are observed at higher binding energies (687-690 eV) and these additional peaks have significantly increased intensity upon prolonged cycling (Fig. 2). The peaks observed at higher binding energies are characteristic of B-F compounds from the decomposition of LiBF$_4$ salt.[36, 37] The changes in peak intensity indicate that the film generated from LiBF$_4$ is not stable during cycling. A corresponding change in atomic concentration is also observed upon cycling where the concentration of B increases and F decreases (Fig. S6). A broad B-F peak is observed in the B 1s spectrum from 191-195 eV characteristic of a combination of B-F and B-O species.[36-41] The

data suggest the film generated from $LiBF_4$ reacts with carbonate solvents to generate B-O-C and B-F containing species after prolonged cycling.

The surface of the lithium electrode plated with the LiBOB electrolyte has a characteristic peak assigned to lithium carboxylate or lithium oxalate at 289 eV, as well as C-O at 286.8 eV in the C1s spectrum (Fig. 2). The corresponding peaks characteristic of C=O and C-O are observed at 531.8 and 533.5 eV, respectively, in the O 1s spectra. The B 1s spectrum contains a peak at 193.5 eV assigned to B-O species.[39-41] The elemental concentration of the surface film on the lithium electrodes plated with the LiBOB electrolyte is dominated by C and O containing species[42], as depicted in Fig. S6.

The XPS spectra of the lithium electrode plated with the LiDFOB and $LiBF_4$+LiBOB electrolytes are very similar for the 1st plating, as both surface films contain lithium carboxylate or lithium oxalate (289 eV, C 1s) along with a C-O peak (286.8 eV, C 1s). Upon additional cycling, the surface film on the lithium electrode cycled with the LiDFOB electrolyte does not change significantly. However, upon additional cycling the surface film on lithium electrode plated with the $LiBF_4$+LiBOB electrolyte changes significantly. After 10 cycles the element spectra and elemental concentrations are very similar to the surface film on lithium electrode cycled with the LiBOB electrolyte (Fig. 2 and Fig. S6). For example, the concentration of F and the intensity of the LiF peak (685 eV, F 1s) decreases considerably after prolonged cycling with the $LiBF_4$+LiBOB electrolyte. Further, the peak assigned to B-O (193.5 eV, B 1s) increases in intensity upon cycling, as observed for the lithium electrode cycled with the LiBOB electrolyte. The results suggest that the LiDFOB and $LiBF_4$+LiBOB electrolytes generate an initial surface film with very similar composition. However, upon cycling, the surface film of the lithium metal electrode cycled with the LiDFOB electrolyte is stable, affording good capacity retention and high efficiency, while the surface film of the lithium electrode cycled with the $LiBF_4$+LiBOB electrolyte is unstable, evolving into a surface film which causes poor efficiency for the lithium metal electrode.

Depth profiling with argon ion-beam sputtering has been performed on cycled lithium electrodes (i.e. at the 10th plating) with the LiDFOB and $LiBF_4$+LiBOB electrolytes (Fig. S7). The electrode cycled with the $LiBF_4$+LiBOB electrolyte contains more C and O and less F than the electrode cycled with the LiDFOB electrolyte. As the sputtering time is increased, the composition of the surface of electrode cycled with the $LiBF_4$+LiBOB electrolyte changes more than the surface of electrode cycled with the LiDFOB electrolyte. This change in atomic concentration upon sputtering suggests that the SEI composition changes as a function of depth, consistent with an SEI composed of primarily of LiBOB decomposition products on the exterior and $LiBF_4$ decomposition products on the interior, as discussed above. The elemental composition of the surface of electrode cycled with the LiDFOB electrolyte, has much smaller changes upon sputtering suggesting that a stable and homogeneous surface film is generated. The

results suggest that the presence of the LiDFOB salt generates favorable and stable SEI on lithium surface which minimizes surface film changes during prolonged cycling.

3.3. Morphology Analysis (TEM)

To understand the morphology of plated lithium and SEI nanostructure, TEM analysis has been conducted on lithium electrodes with representative images and EDX spectra shown in Fig. 3. Since the chemical composition of the surface films are very similar for the LiDFOB and LiBF$_4$+LiBOB electrolytes, the morphology of the surface films has been analyzed to develop a better understanding for the source of the significant performance differences. The morphology was also investigated for the LiPF$_6$ electrolyte for further comparison.

The morphology of plated lithium is dependent on the electrolyte used. Specifically, the appearance of lithium plated from the LiPF$_6$ electrolyte is non-uniform (Fig. 3a). There is no unique morphology observed and many different shapes of lithium (light and dark gray, Fig. 3b) are present on the copper TEM grid (black, Fig. 3b) consistent with the formation of dendritic and mossy lithium. Due to this non-uniformity, the features of the SEI are inconsistent and difficult to resolve.

By comparison, lithium plated from the LiDFOB electrolyte is uniform, smooth, and contains very small particles (5-10 nm) evenly distributed on the surface (Fig. 3c). While most of the small particles are evenly distributed, some of the small particles cluster together to form larger secondary particles. High resolution imaging of the secondary particles reveals that the particles covered by a smooth layer (Fig. 3d). The primary particles have a darker contrast than the outer layer, suggesting that they have a higher atomic number. Analysis of surface of the lithium plated from the LiDFOB electrolyte by EDX (Fig. 3g and h) indicates that the clusters of the primary particles (point 1, secondary particle) are largely composed of F while the surrounding coating (point 2) is largely composed of O. Therefore, the TEM data coupled with the XPS suggest that electrodes cycled with LiDFOB electrolyte have an SEI composed of nanostructured LiF particles covered with a smooth layer of lithium alkyl carbonates, Li$_2$CO$_3$ and lithium oxalate. This also correlates with the argon sputtering investigations with XPS (Fig. S7), which demonstrate that the inner region contains more F than the outer surface. These observations are also consistent with recent exploration of similar SEI structures on lithium metal using the cryogenic TEM technique[43].

Similar LiF-containing particles are also observed on lithium plated from the LiBF$_4$+LiBOB electrolyte, however, the secondary particles are much larger (200-400 nm) than the particles plated from the LiDFOB electrolyte (Fig. 3e), and are not covered by a smooth layer (Fig. 3f). From EDX characterization (Fig. S8), these larger particles have a relatively high concentration of F, while the surrounding area is composed of O. It is suggested that the LiBF$_4$+LiBOB electrolyte is able to generate similar particles, compared to particles generated by the LiDFOB

9

electrolyte. However, the growth of these secondary particles is not controlled upon generation from the LiBF$_4$+LiBOB electrolyte. Given the similar chemical composition of the SEI generated from the LiDFOB and LiBF$_4$+LiBOB electrolytes (15% of 1st plating, Fig. S5), the distribution and size of these nanostructured LiF particles must significantly influence the cycling performance of lithium metal anodes.

3.4. Role of LiDFOB as a Capping Agent

It is proposed that during the reductive decomposition of LiDFOB, the decomposition products, likely oxalate or CO_2 act as a capping agent[44-46] for LiF nanoparticle generation (Fig. 4a and b). Similar capping agents have been widely used for the synthesis of nanoparticles. A capping agent enables control over the size or shape of particles without agglomeration by modifying the surface of particles. Oxalates are one of the typical capping agents used to prepare metal oxide nanomaterials.[47, 48] Therefore, the oxalate moiety of LiDFOB and LiBOB may be functioning as a capping agent to generate nanostructured LiF. LiDFOB contains both fluorine and oxalate moieties (Fig. 4a), enhancing the capping process for LiDFOB compared to LiBOB, since both the LiF and lithium oxalate are derived from reduction of the same molecular structure. This enhanced capping results in the generation of smaller particles (Fig. 4b) from the LiDFOB electrolyte compared to the LiBF$_4$+LiBOB electrolyte. The morphology of the SEI appears to strongly influence the plating and stripping performance of lithium electrodes[7, 49], since the molecular composition of the SEI after the first plating is very similar for the LiDFOB and LiBF$_4$+LiBOB electrolytes (Fig. 2). The presence of an SEI comprised of nanostructured LiF on lithium electrode plated from the LiDFOB electrolyte has dramatically better capacity retention, efficiency and exhibits the smallest impedance.

Based on all the observed data, a model for surface film formation for lithium metal plated with the LiDFOB and LiBF$_4$+LiBOB electrolytes has been proposed as illustrated in Fig. 4c and d. Decomposition of the electrolyte is initiated immediately as the lithium metal is plated. The LiDFOB salt participates in film formation during lithium plating from the LiDFOB electrolyte. Both LiBF$_4$ and LiBOB also participate in film formation for lithium plated with the LiBF$_4$+LiBOB electrolyte. During film formation, LiF particles are generated on the surface of lithium or copper. Effective capping by LiDFOB results in the generation of very small (~5 nm) LiF particles covered by a layer of lithium oxalate or Li_2CO_3 (Fig. 4c). Interestingly, the LiF/Li_2CO_3 interface at the nanostructured level has been computationally predicted to have high lithium ion conductivity which could also contribute to the good performance of the LiDFOB electrolyte.[50] However, when lithium is plated with the LiBF$_4$+LiBOB electrolyte, the size and distribution of the LiF particles is not controlled well due to the poor capping ability of LiBOB compared to LiDFOB. The LiF particles grow much larger and do not evenly coat the surface. In

addition, continuous LiBOB reduction during prolonged cycling generates a more resistive surface film on the lithium electrode which quickly leads to cell failure (Fig. 4d).

The differences in cycling performance can be related to differences in diffusion field gradients at the nanometer scale. Schematic diagrams of the diffusion field on lithium plated with the LiDFOB and LiBF$_4$+LiBOB electrolytes are depicted in Fig. 4e and f. Since LiF has an electronically insulating nature[51] and its cation diffusivity is lower than other SEI components[52], the surface covered with LiF can be considered as an inactive area for lithium plating/stripping. Thus, the surface film on the lithium metal electrode has both active and inactive areas, affecting both electrochemical performance and lithium deposition. Active areas of the electrode generate a lithium diffusion field, and these individual diffusion fields extend over the projected boundaries of the inactive areas. If the size of each inactive area (e.g. LiF) is smaller than a critical dimension, the separated diffusion fields merge into a linear single field[53] (Fig. 4e). Under these conditions, lithium ion diffusion is not hindered by the presence of the inactive areas, having an area equal to the geometric area of the entire surface, even including inactive areas. This phenomenon is commonly observed in ultramicroelectrodes (UMEs)[53-55], which are used in various electrochemical measurements or electrochemical sensors. On the contrary, if the size of each inactive area is larger than a critical dimension (Fig. 4f), the separated diffusion fields do not merge, and the overall diffusion field is hindered by the presence of inactive areas. The disturbance in the diffusion field results in poor efficiency and irregular dendrite growth, due to a non-uniform lithium ion distribution.[56, 57] The differences in diffusion fields provide an explanation for an SEI containing nanostructured LiF particles improving the performance of lithium metal anodes plated from the LiDFOB electrolyte.

4. Conclusions

The common LiBF$_4$, LiBOB, and LiDFOB salts were utilized to understand key mechanisms for improving the cycling performance of lithium metal anodes, providing insight for future electrolyte development. The LiDFOB electrolyte provides a dramatic improvement in electrochemical performance compared to the other salts. However, lithium cycled with the LiBF$_4$+LiBOB electrolyte has rapid performance decay even though it has an equivalent chemical composition to the LiDFOB electrolyte. Ex-situ surface analysis (XPS) suggests that the surface film generated on lithium is primarily composed of lithium alkyl carbonate, Li$_2$CO$_3$, lithium oxalate, and LiF. The initial composition of the surface film generated on lithium with the LiBF$_4$+LiBOB electrolyte is very similar to the composition of the surface film generated on lithium with the LiDFOB electrolyte. However, after 10 cycles with the LiBF$_4$+LiBOB electrolyte the capacity fades and the surface film evolves into a surface film with a similar composition to that observed with the LiBOB electrolyte. This suggests LiBOB is continuously decomposed covering the initially formed unstable SEI on lithium metal electrode. TEM analysis

reveals the LiDFOB electrolyte generates a uniform film composed of nanostructured LiF particles covered by a smooth layer of Li_2CO_3 and lithium oxalate on the lithium surface, while the $LiBF_4$+LiBOB electrolyte generates an inhomogeneous film containing much larger LiF particles which are not homogenously covered by a film of Li_2CO_3 and lithium oxelate. Based on this analysis, the generation of nanostructured LiF particles has been proposed to result from the presence of oxalate based capping agents within the same molecular component as the source of the LiF (LiDFOB). The presence of the nanostructured LiF particles results in the generation of uniform diffusion field gradients which afford uniform lithium plating. Thus, the controlled generation of nanostructured LiF plays a critical role in the improved plating/stripping performance of lithium metal anodes, in addition to the composition of stable SEI generated from the LiDFOB electrolyte. Based on this model, researchers are motivated to pursue new synthetic routes for energy storage materials, applicable not only to liquid organic electrolytes for lithium metal batteries, but for next-generation energy storage systems as well.

Conflicts of Interest

There are no conflicts of interest.

Acknowledgements

Bibliographic References

1. J. S. Dunning, W. H. Tiedemann, L. Hsueh and D. N. Bennion, *J. Electrochem. Soc.*, 1971, **118**, 1886-1890.

2. V. R. Koch, *J. Power Sources*, 1981, **6**, 357-370.

3. E. Peled, *J. Electrochem. Soc.*, 1979, **126**, 2047-2051.

4. Z. Tu, P. Nath, Y. Lu, M. D. Tikekar and L. A. Archer, *Acc. Chem. Res.*, 2015, **48**, 2947-2956.

5. S. Choudhury, A. Agrawal, S. Wei, E. Jeng and L. A. Archer, *Chem. Mater.*, 2016, **28**, 2147-2157.

6. N.-W. Li, Y.-X. Yin, C.-P. Yang and Y.-G. Guo, *Adv. Mater.*, 2016, **28**, 1853-1858.

7. J. Qian, W. A. Henderson, W. Xu, P. Bhattacharya, M. Engelhard, O. Borodin and J. G. Zhang, *Nat Commun*, 2015, **6**, 6362.

8. S. Fang, L. Qu, D. Luo, S. Shen, L. Yang and S.-i. Hirano, *RSC Adv.*, 2015, **5**, 33897-33904.

9. J. Qian, W. Xu, P. Bhattacharya, M. Engelhard, W. A. Henderson, Y. Zhang and J.-G. Zhang, *Nano Energy*, 2015, **15**, 135-144.

10. S. M. Wood, C. H. Pham, R. Rodriguez, S. S. Nathan, A. D. Dolocan, H. Celio, J. P. de Souza, K. C. Klavetter, A. Heller and C. B. Mullins, *ACS Energy Letters*, 2016, **1**, 414-419.

11. J. Zheng, M. H. Engelhard, D. Mei, S. Jiao, B. J. Polzin, J.-G. Zhang and W. Xu, *Nature Energy*, 2017, **2**, 17012.

12. K. Xu, *Chem. Rev.*, 2004, **104**, 4303-4418.

13. E. Markevich, G. Salitra, F. Chesneau, M. Schmidt and D. Aurbach, *ACS Energy Letters*, 2017, **2**, 1321-1326.

14. H. Xiang, P. Shi, P. Bhattacharya, X. Chen, D. Mei, M. E. Bowden, J. Zheng, J.-G. Zhang and W. Xu, *J. Power Sources*, 2016, **318**, 170-177.

15. S. Choudhury and L. A. Archer, *Advanced Electronic Materials*, 2016, **2**, n/a-n/a.

16. X.-Q. Zhang, X.-B. Cheng, X. Chen, C. Yan and Q. Zhang, *Adv. Funct. Mater.*, 2017, **27**, 1605989-n/a.

17. Y. Lu, Z. Tu and L. A. Archer, *Nat Mater*, 2014, **13**, 961.

18. L. Fan, H. L. Zhuang, L. Gao, Y. Lu and L. A. Archer, *J Mater Chem A*, 2017, **5**, 3483-3492.

19. M. Nie, D. P. Abraham, Y. Chen, A. Bose and B. L. Lucht, *The Journal of Physical Chemistry C*, 2013, **117**, 13403-13412.

20.   P. Verma, P. Maire and P. Novak, *Electrochim. Acta*, 2010, **55**, 6332-6341.

21.   H. Buqa, P. Golob, M. Winter and J. O. Besenhard, *J. Power Sources*, 2001, **97-98**, 122-125.

22.   A. M. Andersson and K. Edström, *J. Electrochem. Soc.*, 2001, **148**, A1100-A1109.

23.   H.-G. Steinrück, C. Cao, Y. Tsao, C. J. Takacs, O. Konovalov, J. Vatamanu, O. Borodin and M. F. Toney, *Energy Environ. Sci.*, 2018, **11**, 594-602.

24.   N. Takenaka, Y. Suzuki, H. Sakai and M. Nagaoka, *The Journal of Physical Chemistry C*, 2014, **118**, 10874-10882.

25.   A. Tokranov, B. W. Sheldon, P. Lu, X. Xiao and A. Mukhopadhyay, *J. Electrochem. Soc.*, 2014, **161**, A58-A65.

26.   M. Nie and B. L. Lucht, *J. Electrochem. Soc.*, 2014, **161**, A1001-A1006.

27.   J. Qian, B. D. Adams, J. Zheng, W. Xu, W. A. Henderson, J. Wang, M. E. Bowden, S. Xu, J. Hu and J.-G. Zhang, *Adv. Funct. Mater.*, 2016, **26**, 7094-7102.

28.   Z. L. Brown, S. Jurng and B. L. Lucht, *J. Electrochem. Soc.*, 2017, **164**, A2186-A2189.

29.   E. Kazyak, K. N. Wood and N. P. Dasgupta, *Chem. Mater.*, 2015, **27**, 6457-6462.

30.   F. Wu, J. Qian, R. Chen, J. Lu, L. Li, H. Wu, J. Chen, T. Zhao, Y. Ye and K. Amine, *ACS Applied Materials & Interfaces*, 2014, **6**, 15542-15549.

31.   Q. Xu, Y. Yang and H. Shao, *Electrochim. Acta*, 2018, **259**, 534-541.

32.   B. Qin, S. Zhang, Z. Hu, Z. Liu, J. Zhang, J. Zhao, J. Xiong and G. Cui, *Ionics*, 2017, **23**, 1399-1406.

33.   R. Dedryvère, S. Laruelle, S. Grugeon, L. Gireaud, J.-M. Tarascon and D. Gonbeau, *J. Electrochem. Soc.*, 2005, **152**, A689-A696.

34.   A. M. Andersson and K. Edstrom, *J. Electrochem. Soc.*, 2001, **148**, A1100-A1109.

35.   R. Dedryvere, H. Martinez, S. Leroy, D. Lemordant, F. Bonhomme, P. Biensan and D. Gonbeau, *J. Power Sources*, 2007, **174**, 462-468.

36.   E. A. Il'inchik, V. V. Volkov and L. N. Mazalov, *J. Struct. Chem.*, 2005, **46**, 523-534.

37.   A. M. Andersson, M. Herstedt, A. G. Bishop and K. Edström, *Electrochim. Acta*, 2002, **47**, 1885-1898.

38.   T. Schedlbauer, U. C. Rodehorst, C. Schreiner, H. J. Gores and M. Winter, *Electrochim. Acta*, 2013, **107**, 26-32.

39.   G. V. Zhuang, K. Xu, T. R. Jow and P. N. Ross, *Electrochem. Solid-State Lett.*, 2004, **7**, A224-A227.

40.   E. M. Wigayati, T. Lestariningsih, A. Subhan, C. R. Ratri and I. Purawiardi, *Ionics*, 2016, **22**, 43-50.

41.   T. Lestariningsih, E. Wigayati, C. Ratri and Q. Sabrina, *Journal of Physics: Conference Series*, 2017, **817**.

42.   K. Xu, U. Lee, S. Zhang, M. Wood and T. R. Jow, *Electrochem. Solid-State Lett.*, 2003, **6**, A144.

43.   X. Wang, M. Zhang, J. Alvarado, S. Wang, M. Sina, B. Lu, J. Bouwer, W. Xu, J. Xiao, J. G. Zhang, J. Liu and Y. S. Meng, *Nano Lett.*, 2017, DOI: 10.1021/acs.nanolett.7b03606.

44.   Y. Xia, Y. Xiong, B. Lim and S. E. Skrabalak, *Angewandte Chemie (International ed. in English)*, 2009, **48**, 60-103.

45.   S. Campisi, M. Schiavoni, C. Chan-Thaw and A. Villa, *Catalysts*, 2016, **6**, 185.

46.   C. M. Phan and H. M. Nguyen, *The Journal of Physical Chemistry A*, 2017, **121**, 3213-3219.

47.   S. Vaidya, T. Ahmad, S. Agarwal and A. K. Ganguli, *J. Am. Ceram. Soc.*, 2007, **90**, 863-869.

48.   R. Pegu, K. J. Majumdar, D. J. Talukdar and S. Pratihar, *RSC Adv.*, 2014, **4**, 33446-33456.

49.   K. Yan, H.-W. Lee, T. Gao, G. Zheng, H. Yao, H. Wang, Z. Lu, Y. Zhou, Z. Liang, Z. Liu, S. Chu and Y. Cui, *Nano Lett.*, 2014, **14**, 6016-6022.

50.   Q. Zhang, J. Pan, P. Lu, Z. Liu, M. W. Verbrugge, B. W. Sheldon, Y.-T. Cheng, Y. Qi and X. Xiao, *Nano Lett.*, 2016, **16**, 2011-2016.

51.   M. Gauthier, T. J. Carney, A. Grimaud, L. Giordano, N. Pour, H.-H. Chang, D. P. Fenning, S. F. Lux, O. Paschos, C. Bauer, F. Maglia, S. Lupart, P. Lamp and Y. Shao-Horn, *The Journal of Physical Chemistry Letters*, 2015, **6**, 4653-4672.

52.   L. Benitez and J. M. Seminario, *J. Electrochem. Soc.*, 2017, **164**, E3159-E3170.

53.   A. J. Bard and L. R. Faulkner, *Electrochemical Methods: Fundamentals and Applications, 2nd Edition*, John Wiley & Sons, 2000.

54.   C. G. Zoski, *Electroanalysis*, 2002, **14**, 1041-1051.

55.   K. Aoki, *Electroanalysis*, 1993, **5**, 627-639.

56.   X.-B. Cheng, M.-Q. Zhao, C. Chen, A. Pentecost, K. Maleski, T. Mathis, X.-Q. Zhang, Q. Zhang, J. Jiang and Y. Gogotsi, *Nature Communications*, 2017, **8**, 336.

57.   F. Sagane, K.-i. Ikeda, K. Okita, H. Sano, H. Sakaebe and Y. Iriyama, *J. Power Sources*, 2013, **233**, 34-42.
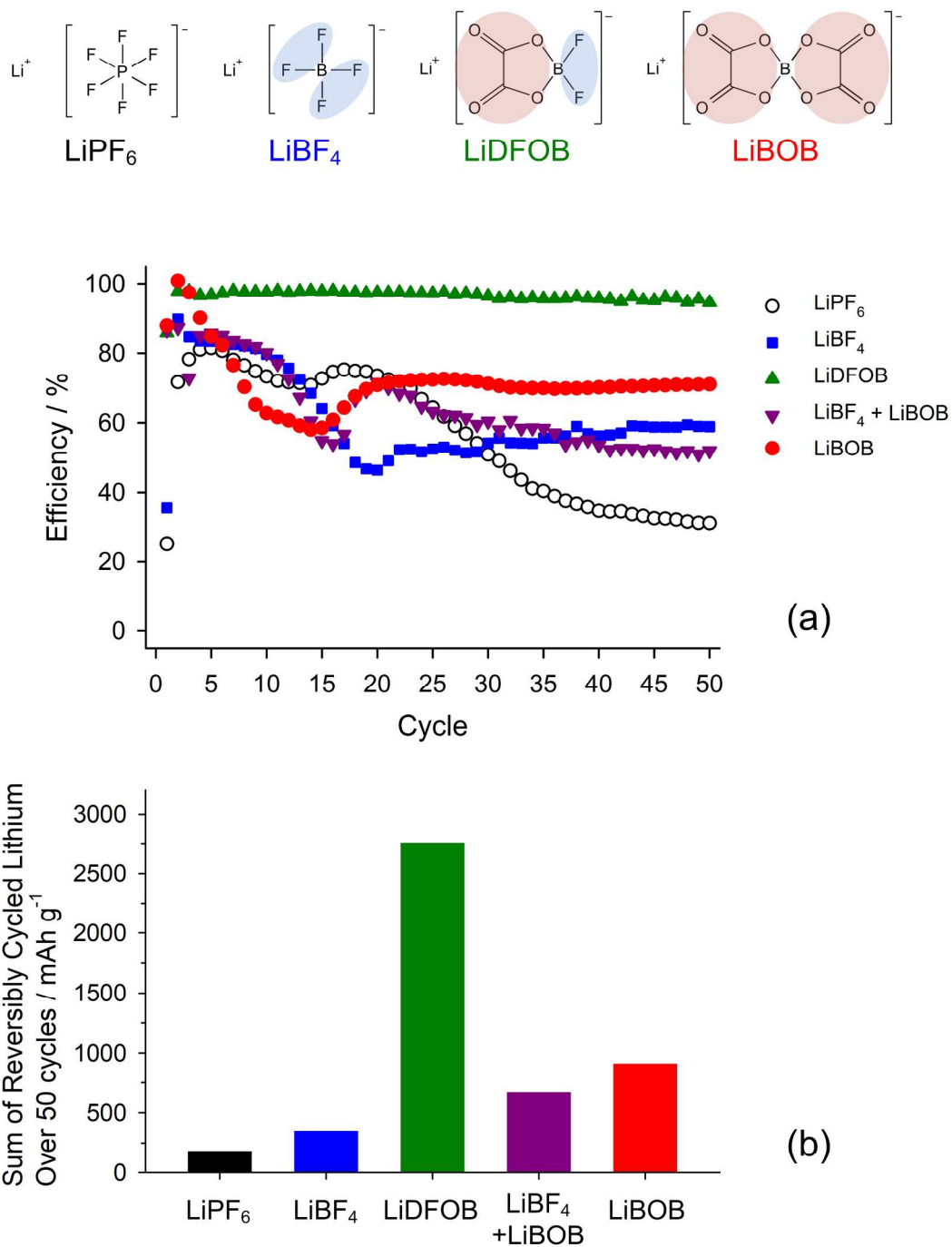
Fig. 1. Comparison of (a) Coulombic efficiency *vs.* cycle number and (b) total sum of reversibly cycled lithium over 50 cycles obtained from LiFePO$_4$/Cu cells.
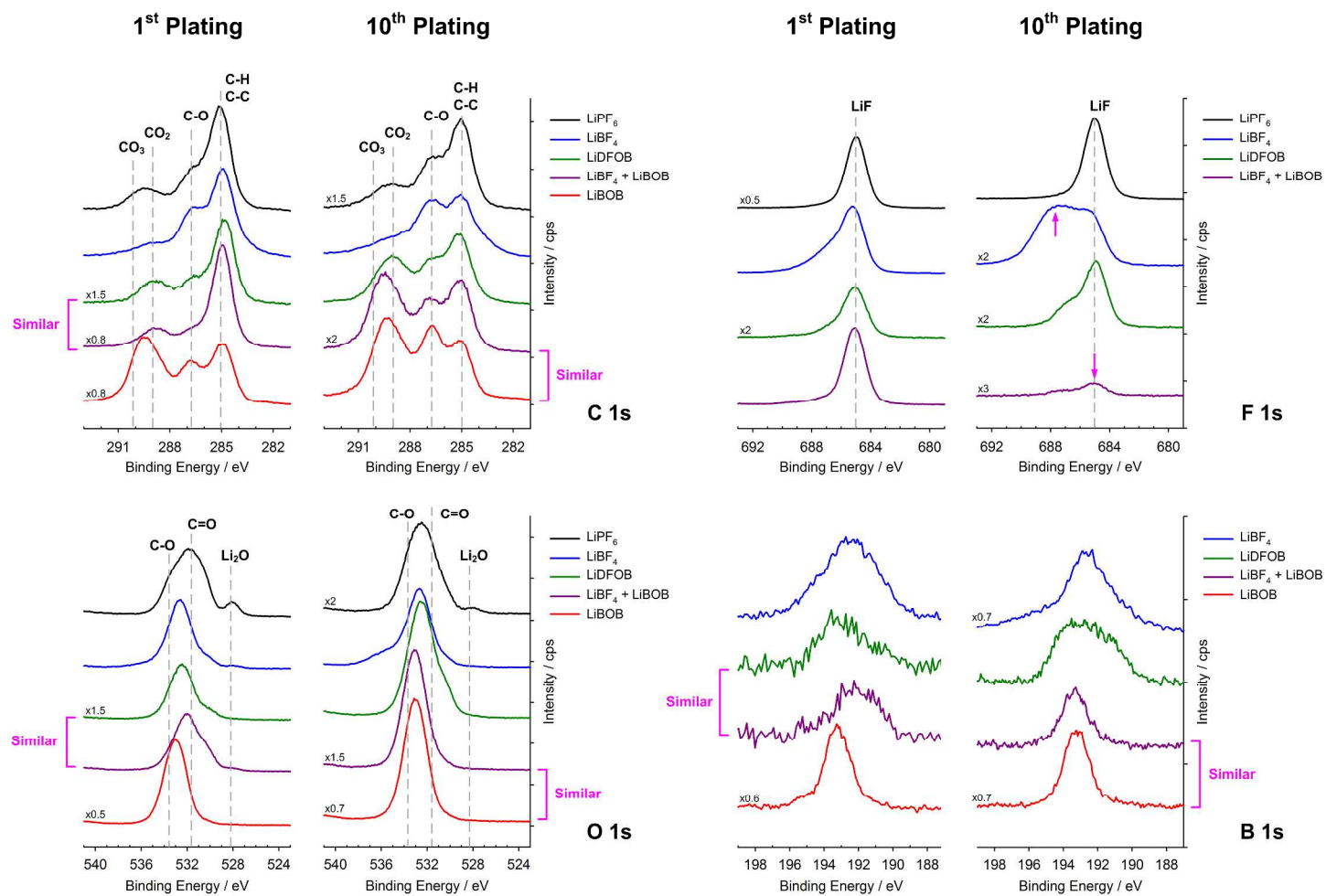
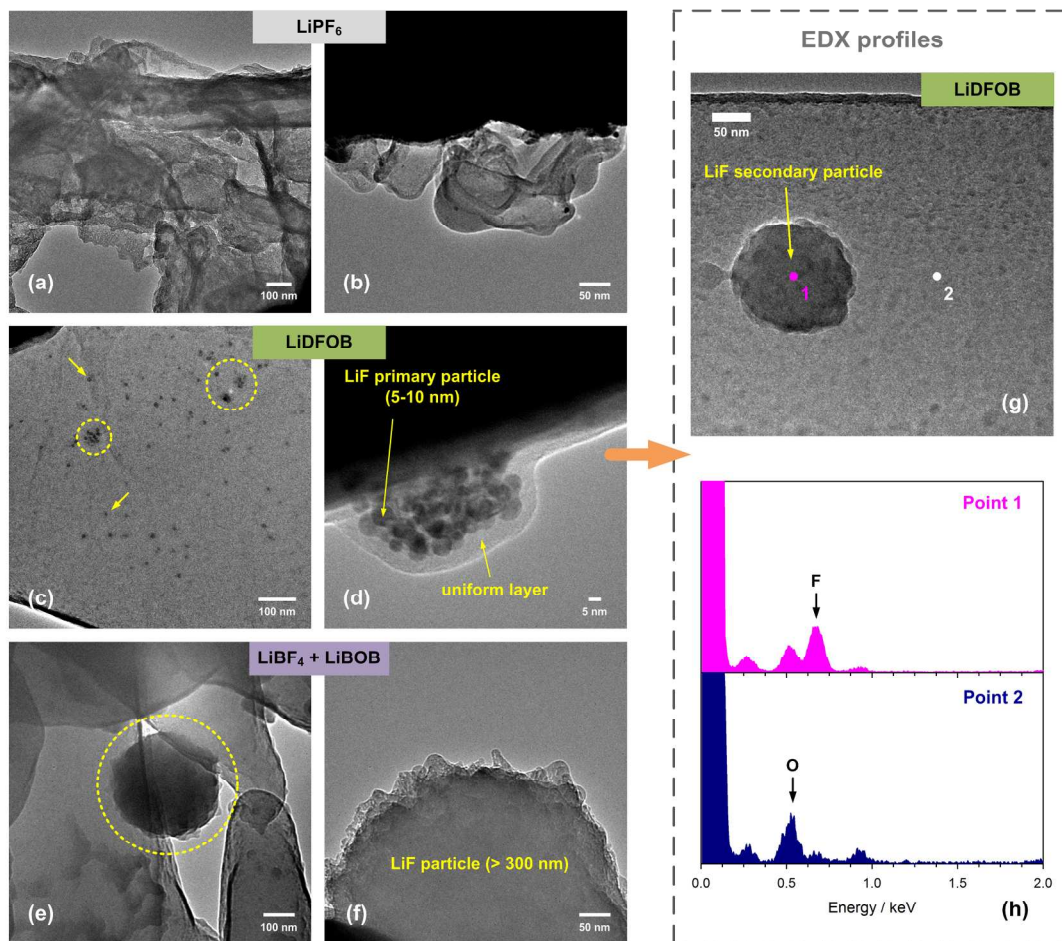Fig. 2. XPS spectra obtained from lithium plated using the investigated electrolytes.

Fig. 3. TEM images of lithium plated from (a, b) 1.2 M LiPF$_6$ in EC:EMC; (c, d) 1.2 M LiDFOB in EC:EMC; (e, f) 0.6 M LiBF$_4$ + 0.6 M LiBOB in EC:EMC and (g, h) EDX spectra of lithium plated from 1.2 M LiDFOB in EC:EMC.
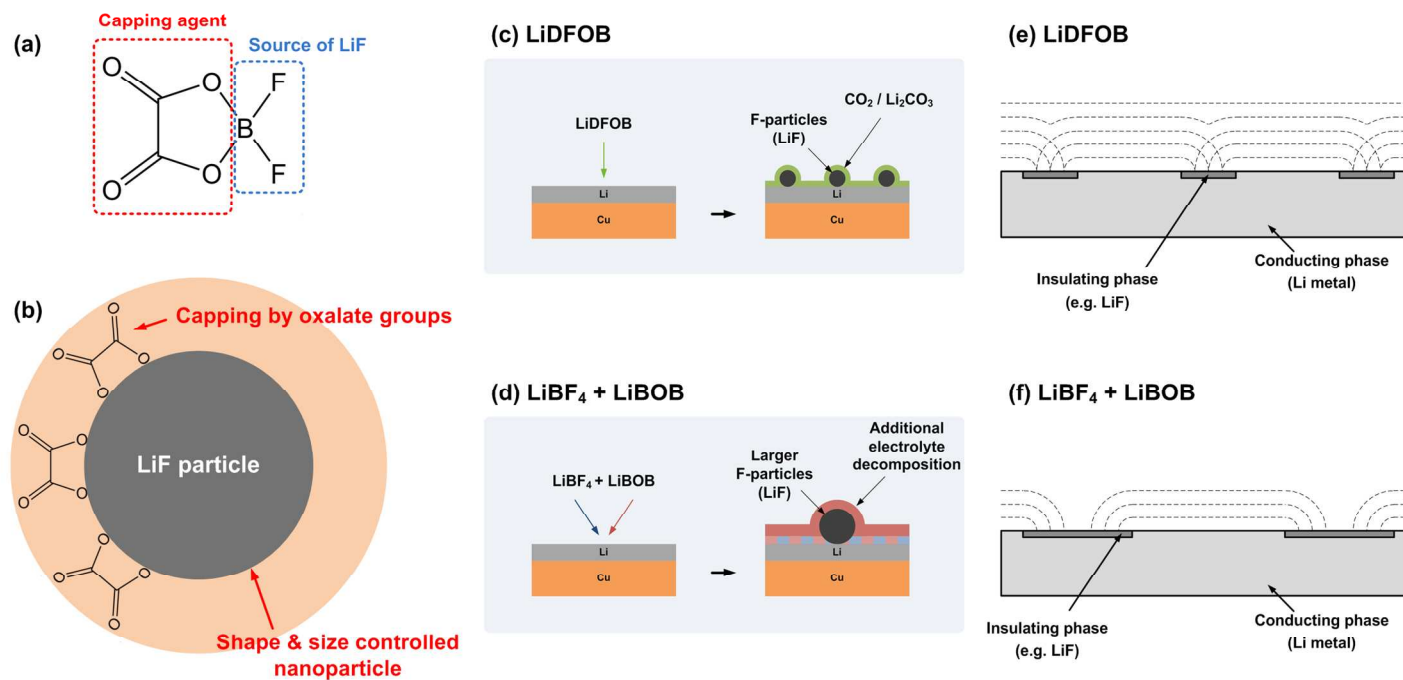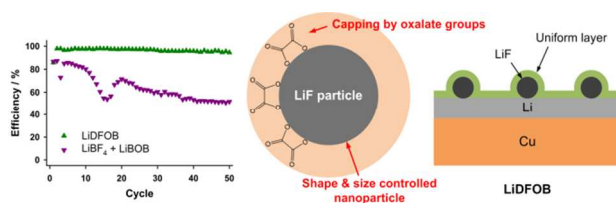
Fig. 4. (a, b) Proposed mechanisms of LiDFOB acting as a capping agent for LiF nanoparticle generation; (c, d) models of SEI from the (c) LiDFOB and (d) LiBF$_4$+LiBOB electrolyte; and (e, f) schematic of diffusion fields at lithium plated from each electrolyte. Each lithium has active and inactive areas on its surface.

Nanostructure of the SEI may be as important as the molecular composition of the SEI for good cycling performance of lithium metal anodes.

Broader Context

Due to its high theoretical capacity and low electrochemical potential, lithium metal is a promising negative electrode material for future high energy density batteries. Unfortunately, commercialization of rechargeable lithium metal anodes is limited by lithium dendrite growth and low Coulombic efficiency. In order to improve the cycling performance, a stable solid electrolyte interphase (SEI) on lithium metal is required. The structure function relationship of the SEI has been investigated using electrolytes with similar molecular composition. The similar electrolytes generate an SEI with similar molecular composition but different nanostructure. The nanostructure of the SEI, not the molecular composition, results in a very large difference in the cycling performance of the cells. This novel concept provides significant new insight for design of the SEI in lithium batteries, especially related to lithium metal anodes. In addition, the manuscript introduces a unique model to explain how LiF, a common component in the SEI and typically a poor lithium ion conductor, can be very beneficial when present as evenly dispersed nanoparticles. The results in this manuscript significantly expand upon the understanding of the SEI and the role of LiF in the function of the SEI.